


Experimental observation and pressure drop modeling of plug formation in horizontal millifluidic hydraulic conveying

Marc Fischer, Etienne Gagnepain, and Guillaume Dumazer *

LGF, UMR No. 5307, Centre SPIN, Mines Saint-Etienne, Université Lyon, 42023 Saint-Etienne, France



(Received 8 January 2024; accepted 29 March 2024; published 24 April 2024)

The hydraulic conveying of glass beads is studied in a horizontal tube. At low flow rates, plugs can be observed moving across the tube, whereas pseudoplugs can be seen at higher flow rates. A statistical analysis of the plugs' and pseudoplugs' velocities and the plugs' lengths observed is conducted. A transition of the propagation speed distribution is established when the crossing over from a plug to a pseudoplug regime is reached, where the peaked plug velocity distribution turns into a uniform pseudoplug velocity distribution. On the other hand, the statistical distribution of plug lengths exhibits a log-normal mathematical shape. The interpretation of the measured pressure drop evolution with the imposed flow rate by means of an effective viscosity shows an apparent shear-thinning effect coming from the dilution of the granular material. This approach provides a predictive tool for pressure drop calculation in the pseudoplug regime.

DOI: [10.1103/PhysRevE.109.044906](https://doi.org/10.1103/PhysRevE.109.044906)

I. INTRODUCTION

In contrast to pneumatic conveying widely used in industry to handle particulate material where solid particles are carried by an airstream, hydraulic conveying relies on the use of liquids such as water to transport solid matter over a given distance. Hydraulic conveying still plays an important role in our industrial world owing to its relatively low cost and lack of significant energy consumption with regard to the large distances it can potentially handle [1]. It is, for example, used to transport coal slurry [2], iron ore [3], phosphates [4], coal combustion products [5], and mineral wastes [6]. Moreover, the study of hydraulic conveying is intimately related to investigations into the transport of sediments in rivers [7,8] and of sediments and sludge within sewers [9,10]. While numerous empirical and semiempirical formulas have been developed for several decades alongside mechanical models [11–13], our understanding of hydraulic conveying remains imperfect, especially when it comes to the optimization of industrial conveying solution [14,15].

According to [1], horizontal hydraulic conveying is characterized by several regimes such as a stationary bed or moving-bed flow, a heterogeneous suspension flow (with a vertical concentration gradient), and finally a pseudohomogeneous suspension flow while the conveying speed increases at a constant solid concentration. Between the stationary-bed and moving-bed flows, we can observe traveling fluctuations of the bed height. In [16] a phenomenological description of various dense regimes was proposed for pneumatic conveying as granular material and pneumatic gas velocity are varied. Several plug flow regimes have been distinguished when the bed height fills locally the entire tube's cross section, forming plugs clearly separated from each other. A slug flow regime

has been mentioned when the granular matter is transported alongside long gas slugs [17] with large fluctuation in the particle concentration. Some authors [1,18] have also mentioned a dune flow regime established from dilute conditions as the fluid velocity is decreased. Granular heaps have been seen to form and travel at the surface of the granular bed driven by a saltation phenomenon. In geosciences dunes have been studied in detail and a solid physical framework explaining the dune displacement speed as well as dune wavelength can be found in the literature [19,20]. Physical phenomena responsible for the displacement of granular particles at the surface of the bed due to viscous drag by the flowing fluid above are identical when it comes to describing the transport of sand particles by the wind or industrial particulate material in a pneumatic conveying line. However, the geometrical confinement existing in a hydraulic or pneumatic conveying pipe starts to make a major difference when solid particles accumulate so that the tube's or pipe's cross section is filled. For this reason the knowledge successfully developed for understanding dune formation and displacement at the surface of the earth does not apply for dense regimes developing in pneumatic or hydraulic conveying.

Horizontal hydraulic and pneumatic conveying have much in common, so insights into one of the processes can often be profitably used for investigations of the other process [15,21,22]. A large variety of pneumatic conveying regimes exists [17] and the fluid superficial velocity and transported mass rate represent controlling parameters. In both hydraulic and pneumatic conveying, the relationship between pressure drop and superficial gas velocity has been established empirically for a series of mass rate values for a given particulate material and a conveying line [21]. For small superficial gas velocities, the solid friction between solid particles and conveying line walls is the dominant dissipative phenomenon and solid particles agglomerate. In these so-called dense flow regimes, solid particles agglomerate into granular waves, also

*guillaume.dumazer@emse.fr

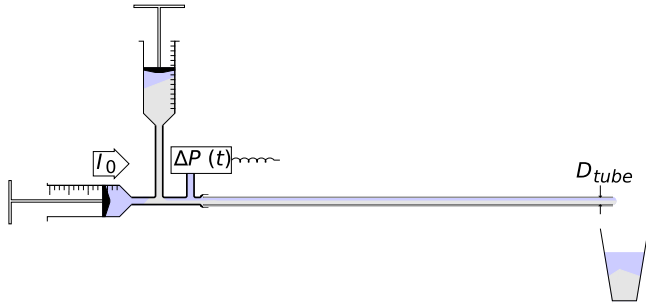


FIG. 1. Sketch of the experimental setup. A horizontal glass tube of inner diameter D_{tube} contains a mixture of water and grains. A syringe pump imposes a constant flow rate of water I_0 and a second syringe filled with glass beads introduces the granular material into the stream at the tube's inlet, where a pressure sensor is returning the measurement $\Delta P(t)$.

called plugs. It has been shown due to tracers that particle speed is lower than the granular wave speed [23]. A pick-up mechanism takes place where solid particles are collected at the front of the propagating plug and are transported over a given distance before being deposited at the rear of the plug and left behind [24,25]. Although less investigated, studies have shown that hydraulic conveying relies on a saltation mechanism, as observed experimentally [26], as well as on a pick-up mechanism [27,28]. Similarly to what has been extensively studied in pneumatic conveying systems, hydraulic conveying crosses over from dense to dilute flow regimes [29] and pressure drop prediction has been approached numerically [15,29].

On the other hand, for particle-laden flows, rheological studies of suspension have provided powerful descriptions of the complex relationship between shear stress with shear rate and solid particle concentration [30,31]. A broad range of dry granular flow or granular suspension can find a useful interpretation due to recent rheological approaches in geosciences [32] or the treatment of industrial issues [33].

In the present study, we investigate the horizontal hydraulic conveying of small glass beads at relatively low flow rates in order to improve our knowledge and comprehension of hydraulic conveying dense regimes in a millifluidic setting. In Sec. II we present our experimental methodology. We show the results of our analysis of the appearance, behavior, and features of plugs and pseudoplugs in Sec. III. In Sec. IV we describe our treatment and analysis of the pressure drop profiles. We conclude this article with a summary and an outlook for further work in Sec. V.

II. EXPERIMENTAL SETUP

The experimental setup can be seen in Fig. 1. The hydraulic transport of a granular phase is obtained experimentally by means of a syringe pump (Harvard apparatus) imposing a fixed flow rate I_0 of filtered water in a millifluidic tube of 590 mm length. A second syringe filled with glass beads of diameter $d_{\text{grain}} \in [70\text{--}110] \mu\text{m}$ is used as a granular reservoir connected to the tube's inlet. The granular matter falls by gravity into the stream of water coming from the syringe pump. A differential pressure sensor (Keller PD-23/8666.1)

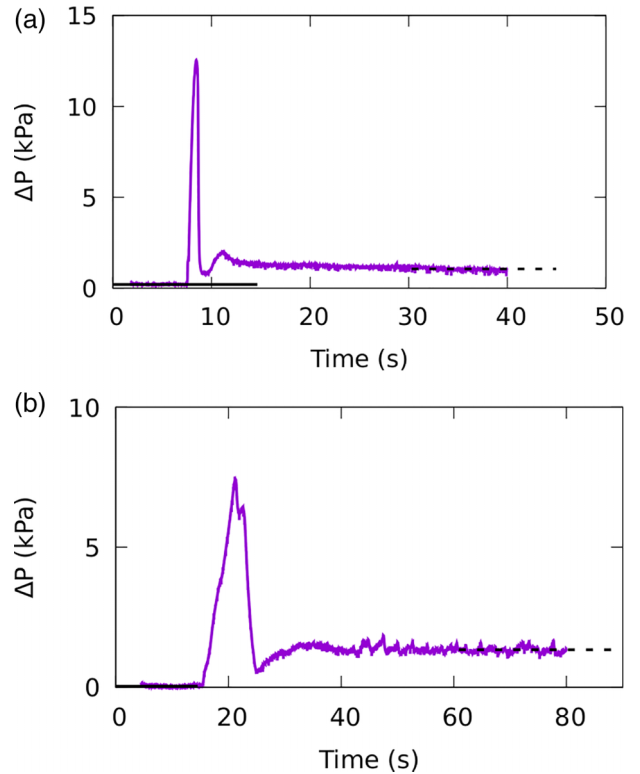


FIG. 2. Pressure time series measured with imposed flow rates (a) $I_0 = 10 \text{ mL min}^{-1}$ and (b) $I_0 = 2 \text{ mL min}^{-1}$. The solid and dashed lines mark the steady-state pressure plateaus obtained without any grains and with grains, respectively.

measures the pressure drop ΔP between the tube's inlet and the atmosphere. The flow inside the tube is recorded by a camera with a frequency of 30 frames per second. The experiments begin by setting up a steady flow containing only water. The granular matter is then poured at a constant rate into the stream of water ahead of the tube's inlet by opening a valve. The tube is initially empty of grains and the natural filling process leading to the formation of a uniform layer of sedimented grains requires a long time before completion. In order to accelerate the relaxation towards a steady hydraulic transport of grains, a quick granular flow is applied by pressing the syringe storing the granular matter. Once a rapid flow of suspended grains is obtained along the entire length of the tube, the pressure on the syringe storing the grains is released and the suspension flow slows down. The suspended granular phase then sediments homogeneously in the tube. This experimental manipulation accounts for the pressure peak visible between the first plateau (corresponding to the Hagen-Poiseuille flow of pure water) and the second plateau (corresponding to the hydraulic transport of granular matter), as can be viewed in Fig. 2. The experiment ends when the water syringe pump is empty. The following flow rate values have been used: 1, 2, 3, 4, 5, 10, 15, and 20 mL min^{-1} . The reproducibility of the observations has been assessed by performing each experiment three times. The present setup imposes a fixed mass rate of grains, since the vertical syringe storing the granular matter can be either closed or fully opened.

The experiments were then systematically recorded with a camera. The image treatment procedure is illustrated in Fig. 3.

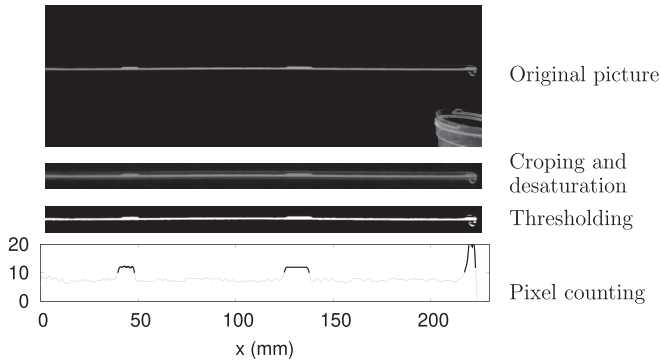


FIG. 3. Image of the treatment procedure applied to the original picture for $I_0 = 1 \text{ mL min}^{-1}$.

First the images are cropped and desaturated. A light intensity threshold is then employed to obtain a black and white picture, whereby the white areas indicate the presence of the white glass beads. For each abscissa x along the horizontal axis and at each time t , the height of granular matter, i.e., the number of white pixels, is calculated. This number is then converted into a black-and-white light intensity. The local amount of grains at a position x is thus converted into a gray scale where light values correspond to large heights of grains, whereas dark values correspond to small heights of grains and eventually, for black values, to the absence of grains. The temporal dynamics is then represented by means of a spatiotemporal diagram as shown in Fig. 4. All granular profiles along the tube obtained after image treatment are stacked on top of each other from the top to the bottom as a function of time. Accordingly, the ordinate corresponds to the temporal axis developing downward, whereas the abscissa corresponds to the longitudinal coordinates.

At the temperature in our laboratory (which fluctuates between 21°C and 24°C), we can take the following values for the density and dynamic viscosity of water: $\rho_w = 997.62 \text{ kg/m}^3$ and $\mu_w = 9.33 \times 10^{-4} \text{ Pa s}$.

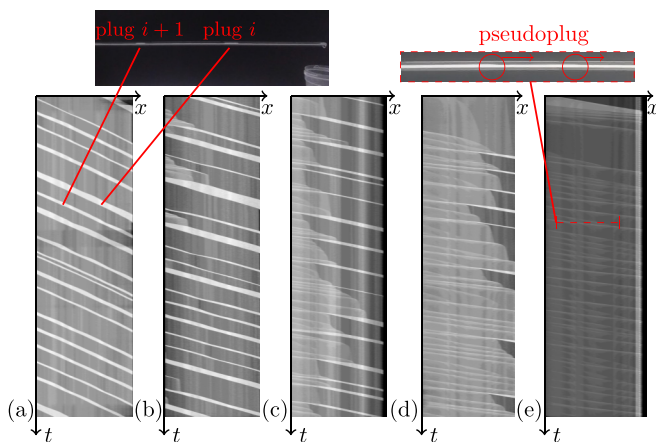


FIG. 4. Spatiotemporal diagrams obtained from a section of the tube of length 234 mm located left of the tube outlet for the following flow rate values: (a) $I_0 = 1 \text{ mL min}^{-1}$, (b) $I_0 = 2 \text{ mL min}^{-1}$, (c) $I_0 = 3 \text{ mL min}^{-1}$, (d) $I_0 = 4 \text{ mL min}^{-1}$, and (e) $I_0 = 5 \text{ mL min}^{-1}$. Time goes downward for 231 s.

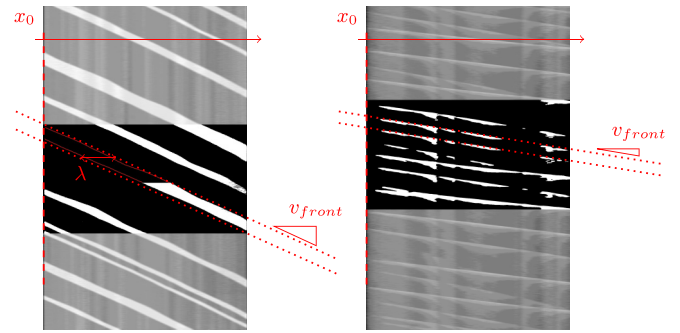


FIG. 5. Details of the spatiotemporal diagram obtained for a flow rate $I_0 = 1 \text{ mL min}^{-1}$ for 85 s (left) and $I_0 = 5 \text{ mL min}^{-1}$ for 79 s (right). Thin red solid lines show the boundaries of the central white stripe after thresholding and contour detection for plugs traveling (left). The two upper and lower slopes in dotted lines indicate the front and the rear velocities, respectively, of the traveling plug. Only the front velocity v_{front} is considered in this work. The plug's length λ is obtained as the distance between the two front- and rear-velocity slopes. For pseudoplug propagation (right), only front velocities v_{front} can be defined.

III. PLUG ANALYSIS

A. Plug and pseudoplug flow regimes

In these experiments we can observe the formation and propagation of plugs for flow rate values $I_0 \leq 3 \text{ mL min}^{-1}$. These plugs correspond to accumulated granular matter filling the tube from bottom to top over a certain length and moving in the flow direction (see the inclined white stripes in the spatiotemporal diagram in Fig. 4).

At higher flow rates $I_0 \geq 3 \text{ mL min}^{-1}$ the sedimented bed appears to be dragged along the tube with no clear plug formed. However, the spatiotemporal analysis shows that granular fronts with small amplitude are traveling. These displacements are evidenced by inclined lines in the spatiotemporal diagrams obtained for $I_0 \geq 4 \text{ mL min}^{-1}$ and are only partially visible in the ones obtained for $I_0 \in [2-3] \text{ mL min}^{-1}$. These lines indicate that some fluctuations of the granular layer's height are propagating from left to right. These propagating fluctuations of the granular matter height will be referred to as pseudoplugs in the rest of the paper.

The first quantity that can be measured from the spatiotemporal diagram is then the plugs' or pseudoplugs' propagation speed v_{front} obtained from the slopes of their stripes (see Fig. 5). We also looked at the plugs' length λ . Note that in the case of pseudoplugs with no clearly defined extensional size, a single velocity v_{front} is measured and no length can be defined in this case.

B. Statistical methodology

As can be seen in Figs. 3 and 4, for flow rates lower than 3 mL min^{-1} , plugs can be observed moving through the tube. However, for $I_0 \geq 3 \text{ mL min}^{-1}$, it becomes harder and harder to identify plugs; concurrently pseudoplug events become more frequent.

As a preliminary verification we performed a Mann-Whitney U test in order to ensure the similarities of the

TABLE I. Mann-Whitney U tests for the plug lengths λ done for a series of observations performed at flow rates $I_0 = 1$ and 2 mL min^{-1} .

I_0 (mL min^{-1})	Trials	$\mathcal{M}(\lambda)$	$q_{25}(\lambda)$	$q_{75}(\lambda)$
1–1	trial 1 to trial 2	3.90×10^{-1}	3.80×10^{-1}	3.50×10^{-1}
1–2	trial 1 to trial 3	9.51×10^{-4}	1.85×10^{-3}	2.95×10^{-4}
1–2	trial 1 to trial 4	3.65×10^{-3}	5.29×10^{-3}	3.02×10^{-3}
1–2	trial 2 to trial 3	4.03×10^{-5}	1.06×10^{-4}	2.10×10^{-5}
1–2	trial 2 to trial 4	8.29×10^{-4}	1.07×10^{-3}	5.37×10^{-4}
2–2	trial 3 to trial 4	2.79×10^{-1}	2.31×10^{-1}	1.91×10^{-1}

statistical properties of random variables such as the plugs' or pseudoplugs' velocities v_{front} and plugs' lengths λ obtained for two different experiments with the same flow rate value. For every plug moving throughout the tube, we computed the three quartiles of the plug's length, i.e., $q_{25}(\lambda)$, $\mathcal{M}(\lambda)$, and $q_{75}(\lambda)$, which are themselves random variables as they can vary from plug to plug. In order to test the similarity of the distribution of a random variable Y during two trials conducted under the same conditions, the Mann-Whitney U test considers the null hypothesis H_0 , $p(Y_1 < Y_2) = p(Y_1 > Y_2)$, against the hypothesis H_1 that $p(Y_1 < Y_2) \neq p(Y_1 > Y_2)$ at least for some values [34]. The results of the Mann-Whitney U test are shown in Table I. The experiments were conducted at an imposed flow rate $I_0 = 1 \text{ mL min}^{-1}$ (trials 1 and 2) and for two series of observations at an imposed flow rate $I_0 = 2 \text{ mL min}^{-1}$ (trials 3 and 4). If the value of the test becomes lower than a risk threshold set to $\alpha = 0.05$, we have a quantitative sign that the two sets of observations may come from different statistical distributions as the probability of obtaining the results we see if the probability distributions are the same (hypothesis H_0) is smaller than α . The highest test values are obtained here for observations made with similar flow rate conditions, i.e., for trials 1 and 2, on the one hand, and for trials 3 and 4, on the other hand. This confirms that we can safely analyze together the results of two observations obtained at the same flow rate.

The cumulative probability distribution function (CDF) of a random variable X is defined as $F(x) = p(X \leq x)$, i.e., the probability that X takes on a value that is equal to or smaller than x . If we know n realizations of the random variable X , the empirical cumulative probability distribution function is defined as

$$F_n(x) = \frac{\mathcal{N}}{n} = \frac{1}{n} \sum_{i=1}^n \mathbf{1}_{\{x_i \leq x\}}, \quad (1)$$

where \mathcal{N} is the number of observations in the sample less than or equal to x . Here $F_n(x)$ converges towards $F(x)$ when n tends to infinity.

C. Results of the statistical analysis

1. Plug and pseudoplug velocities

The velocities are measured from spatiotemporal diagrams. The velocity corresponds to a random variable because it will vary from plug to plug in an unpredictable fashion. Then $\mathcal{M}(v_{\text{front}})$ is the median value of v_{front} when all the plugs observed at the same flow rate are considered. Empirical

cumulative functions for the plugs' and pseudoplugs' velocities present a clear difference [see Fig. 6(a)]. Plugs progress with very narrow velocity distributions, exhibiting little variations as shown by the steep step in the cumulative functions [solid lines in Fig. 6(a)]. Pseudoplugs present conversely some variations of their velocities from pseudoplug to pseudoplug. The almost linear behavior of the cumulative functions for pseudoplug velocities points to a uniform pseudoplug velocity distribution between two extreme values approximately equal to $\frac{1}{2}\mathcal{M}(v_{\text{front}})$ and $\frac{3}{2}\mathcal{M}(v_{\text{front}})$. Both plug and pseudoplug propagation dynamics appear to be determined by a single

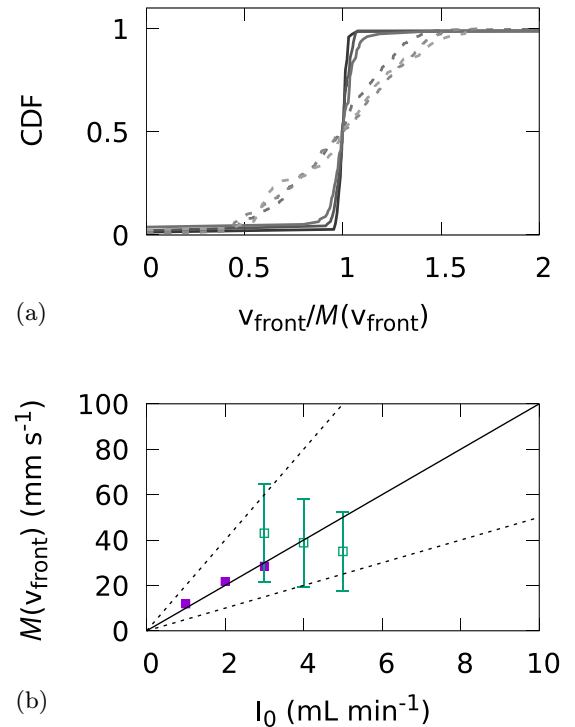


FIG. 6. (a) Empirical cumulative functions for plug (solid lines) and pseudoplug (dashed lines) velocities normalized by the median velocity of each distribution. The shade of gray indicates the imposed flow rate ranging from 1 mL min^{-1} (dark gray) to 5 mL min^{-1} (light gray). (b) Median velocity values of plugs (closed squares) and pseudoplugs (open squares) obtained for different imposed flow rate values. Error bars associated with pseudoplug median velocities correspond to the observed minimal and maximal velocity values. The lines are a guide for the eye, giving the expected fluid velocity averaged over the cross-sectional full aperture (bottom dashed line), 50% aperture (solid line), and 25% aperture (top dashed line).

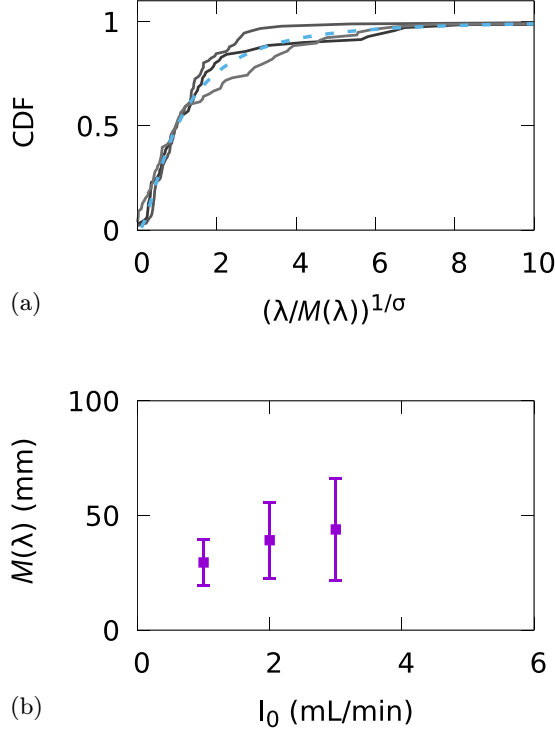


FIG. 7. (a) Normalized empirical cumulative functions of the plug length $[\lambda/M(L)]^{1/\sigma}$ (solid lines) and normalized cumulative function for a log-normal distribution (dashed line). The shades of gray gives the flow rate values ranging from 1 mL min⁻¹ (dark gray) to 3 mL min⁻¹ (lighter gray). (b) Median and variance values used for normalization, represented by closed squares and error bars, respectively.

parameter, i.e., the median propagation velocity, as shown by the collapse of cumulative functions obtained for the plugs, i.e., for $I_0 \in [1-3]$ mL min⁻¹, and for the pseudoplugs, i.e., for $I_0 \in [3-5]$ mL min⁻¹. The evolution of $\mathcal{M}(v_{\text{front}})$ for various imposed flow rates is shown in Fig. 6(b). Plugs have a median velocity increasing with the imposed flow rate. The solid line in Fig. 6(b) is a guide to the eye, showing how the average fluid velocity increases linearly with the flow rate if half of the tube cross section is obstructed by sedimented grains. This average velocity seems to be a fairly good estimate for the plugs' velocities. Pseudoplugs exhibit a counterintuitive behavior with a propagation velocity decreasing with the imposed flow rate. However, their values stay within some limits given by the average fluid velocity in a fully open and a 25% open cross section. This decreasing behavior could correspond to a decreasing obstruction of the tube's cross section due to the sedimented bed erosion increasing with the imposed flow rate. The tube's increasing cross-sectional aperture leads to a decreasing fluid velocity displacing pseudoplugs.

2. Plug lengths

As for plug and pseudoplug velocities, the plug length λ is measured from spatiotemporal diagrams and corresponds to a random variable as it varies from plug to plug. Its median value is denoted by $\mathcal{M}(\lambda)$. Figure 7(a) shows the empirical cumulative function of the plug lengths λ for $I_0 = 1, 2,$ and

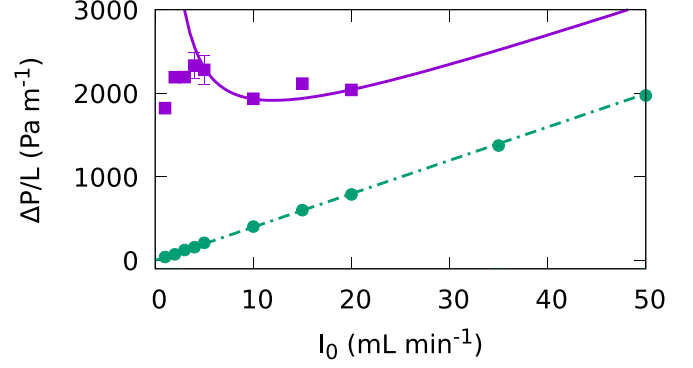


FIG. 8. Pressure drop measurements for pure water (green circles) and for hydraulic conveying of glass beads (purple squares) as a function of the imposed flow rate I_0 . Each experiment was executed two to three times and the error bars show the minimum and maximum measurements. The purple solid line gives the expected pressure drop for a suspension with the Maron-Pierce correlation and a flow-rate-dependent solid filling fraction. The green dash-dotted line gives the expected pressure drop obtained with the Hagen-Poiseuille formula for pure water.

3 mL min⁻¹. The plug length dimensionless variable $\lambda^* = [\lambda/M(\lambda)]^{1/\sigma}$ is obtained from the median value of the plug lengths $\mathcal{M}(\lambda)$ and from the log-normal distribution parameter $\sigma = \sqrt{2\{\ln(\langle\lambda\rangle) - \ln[\mathcal{M}(\lambda)]\}}$, with $\langle\lambda\rangle$ the plug length mean value. An increase of the median plug length $\mathcal{M}(\lambda)$ and of the standard deviation of the distribution can be observed with the imposed flow rate I_0 [see Fig. 7(b)].

The observed plug length distributions for $I_0 \in [1-3]$ mL min⁻¹ fluctuates around the normalized log-normal distribution. The asymptotic distribution of a random splitting process corresponds to a log-normal shape [35,36]. This observation could lead to further modeling assumption about the plug formation mechanism.

IV. PRESSURE DROP ANALYSIS

Evolution of pressure drop

Pressure measurement time series during one experiment show two plateaus separated by a sudden pressure drop peak corresponding to the experimental manipulation leading to the uniform introduction of the granular material into the tube (see Fig. 2). The first plateau corresponds to the pressure drop due to the pure water flow along the tube at a given flow rate I_0 . The final plateau corresponds to the pressure drop resulting from the hydraulic conveying of granular matter. One can observe the increase in pressure drop from pure water flow to hydraulic conveying.

As can be seen in Fig. 8, the pressure drop measurements for pure water (green circles) follow the Hagen-Poiseuille formula (green dash-dotted line)

$$(\Delta P/L)_{\text{HP}} = \frac{128\mu_w I_0}{\pi D_{\text{tube}}^4}. \quad (2)$$

Experiments were executed two to three times to test the reproducibility of the measurements. For each imposed flow rate value, error bars show the maximum and minimum values and

squares are located at the mean values. After granular matter is introduced in the flow, an increase in the pressure drop is observed for every imposed flow rate value. The relative difference between the pressure drop for pure water and for granular matter conveying is however decreasing.

In this system a competition exists between the gravitational force leading to the sedimentation of the granular matter on the bottom of the tube and the viscous drag leading to the conveying of the granular matter along the tube. So we propose to build a dimensionless velocity from the ratio between the mean pure fluid velocity in the tube in the absence of grains $v_G = 4I_0/\pi D_{\text{tube}}^2$ and the sedimentation velocity of a single grain in the fluid $v_{\text{sed}} = \Delta\rho g d_{\text{grains}}^2/18\mu_w$:

$$v_G^* = \frac{72I_0\mu_w}{\pi D_{\text{tube}}^2 \Delta\rho g d_{\text{grains}}^2}. \quad (3)$$

We also suggest consideration of the pressure drop measurements $(\Delta P/L)_{\text{meas}}$ when granular matter is introduced as a perturbation to the nominal pressure drop $(\Delta P/L)_{\text{HP}}$ for pure water given by the Hagen-Poiseuille formula (2). So we consider the reduced pressure drop

$$\left(\frac{\Delta P}{L}\right)^* = \frac{(\Delta P/L)_{\text{meas}} - (\Delta P/L)_{\text{HP}}}{(\Delta P/L)_{\text{HP}}}.$$

Figure 9(a) shows the evolution of the reduced pressure drop, which gives the relative increase with respect to the pressure drop for pure fluid. The measurements made with pure fluid agree with the prediction from the Hagen-Poiseuille formula (2), whereas the measurements made in hydraulic conveying conditions asymptotically converge towards the Hagen-Poiseuille prediction for large velocities v_G^* . On the contrary, the reduced pressure drop seems to diverge as v_G^* tends to zero.

Figure 9(b) shows the evolution of the effective viscosity μ_{eff} divided by the nominal water viscosity. The effective viscosity μ_{eff} corresponds to the viscosity value required so that the Hagen-Poiseuille formula's prediction corresponds to the pressure drop measurements

$$\mu_{\text{eff}} = \left(\frac{\Delta P}{L}\right)_{\text{meas}} \frac{\pi D_{\text{tube}}^4}{128I_0}. \quad (4)$$

The hydraulic conveying pressure drop's asymptotic trend towards the Hagen-Poiseuille prediction could be explained by the decreasing filling fraction in solid materials obtained for large flow rates. Indeed, the solid mass rate w is determined by the tubing and granular material reservoir syringe diameters, which do not change with the flow rate I_0 . A rapid modeling of the filling fraction ϕ could be derived from these two parameters,

$$\phi = \frac{w/\rho_g}{w/\rho_g + I_0}, \quad (5)$$

with the solid volume rate w/ρ_g and the fluid volume rate I_0 . The effective viscosity of a suspension is an increasing function of the filling fraction in solid material [30,31]. In particular, the Maron-Pierce correlation [30] gives a satisfying match to experimental pressure drop measurements and numerical modeling of a relatively simple mathematical formula

$$\mu_{\text{eff}}/\mu_w = (1 - \phi)^{-2}. \quad (6)$$

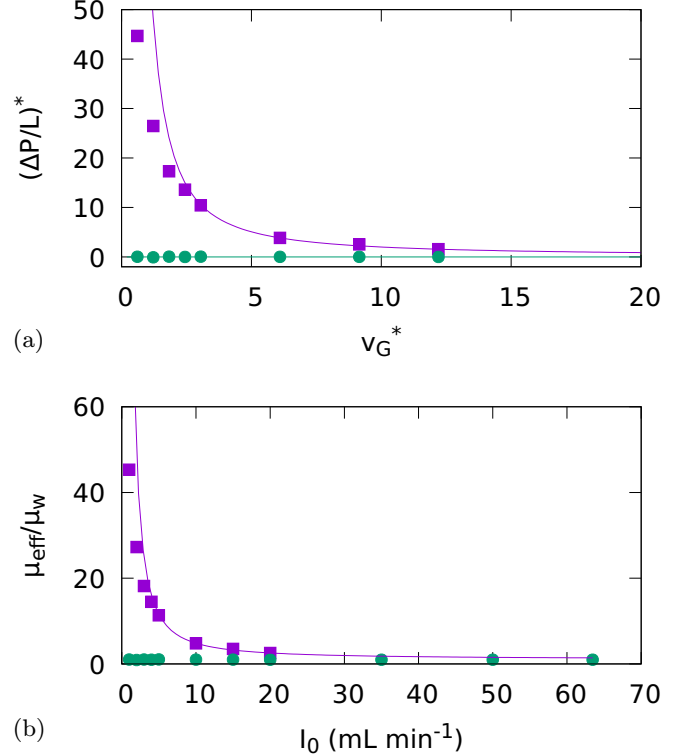


FIG. 9. (a) Reduced pressure drop $(\Delta P/L)^*$ as a function of the dimensionless velocity v_G^* for pure water (green circles) and granular conveying (purple squares). The solid line shows the zero-ordinate baseline Hagen-Poiseuille prediction. (b) Effective viscosity ratio, calculated from the pressure drop measurement μ_{eff} with pure fluid (green circles) and with granular conveying (purple squares), to the nominal fluid viscosity μ_w as a function of the imposed flow rate I_0 . The solid line shows the effective viscosity ratio given by the Maron-Pierce correlation with our flow-rate-dependent filling fraction model.

Putting together Eqs. (5) and (6), an analytical formula can be derived to predict the observed pressure drop measurements in our system:

$$\left(\frac{\Delta P}{L}\right)_{\text{MP}} = \frac{128I_0}{\pi D_{\text{tube}}^4} \mu_w \left(1 - \frac{w/\rho_g}{w/\rho_g + I_0}\right)^{-2}. \quad (7)$$

This formula reproduces the observations for hydraulic conveying with rather good accuracy [see the solid line in Fig. 9(b)]. For flow rate values $I_0 \geq 3$ mL min⁻¹, the decreasing concentration in granular matter leading to a decreasing effective viscosity is well captured by Eq. (7). For lower flow rate values $I_0 \leq 3$ mL min⁻¹ the prediction overestimates the measurements. Although Eq. (7) provides here a very satisfying prediction for the pressure drop in nearly homogeneous horizontal hydraulic conveying from very dilute conditions at high flow rates down to semidense conditions with traveling pseudoplugs, the heterogeneous traveling plug structure may be based on other physical phenomena.

A better estimation of the effective viscosity and pressure drop in the plug regime would require a better modeling of the various dissipative processes in heterogeneous hydraulic conveying (see [37]). The pressure drop increase with

the imposed flow rate observed in the plug regime is consistent with the Ergun equation derived for flow through packed columns [38]. The pressure drop increase indicates then that the fluid is flowing with a faster velocity than the plug speed.

V. CONCLUSION AND OUTLOOK

While heterogeneous dense solid flows in hydraulic conveying systems present the advantage of causing less attrition and erosion than nearly homogeneous dilute flows, they are not as well understood as the latter in part due to the complex frictional interaction with the confining walls. The purpose of the present study was to improve our understanding of these dense flow regimes and their transition towards dilute regimes. The hydraulic conveying of glass beads in a millifluidic tube was investigated through the systematic measurements of the pressure drop and the production of spatiotemporal diagrams from video recording. A full-fledged plug flow regime can be seen at a flow rate of $I_0 \in [1-3]$ mL min⁻¹, whereas a pseudoplug propagation regime is exhibited at flow rates $I_0 \geq 3$ mL min⁻¹.

For the lowest flow rate values here $I_0 \leq 3$ mL min⁻¹ the Archimedes number $Ar = 14.7$ and the particle's Reynolds number $Re \leq 1.6$ would correspond to a plug-1 regime according to [16]. However, the phenomenology observed here does not really match this particular regime as the plug-1 type is supposed to travel across and leave behind its passage an empty tube. In our observations the phenomenology of the observed plugs is closer to the plug-2 type despite the small Archimedes number value. The difference between gas flow used in pneumatic conveying and the liquid flow used in the present hydraulic conveying study probably explains this inconsistency. For larger flow rates $I_0 \geq 3$ mL min⁻¹ the Reynolds number $Re \geq 1.6$ for the same Archimedes number value points towards a so-called dune regime in the literature. This regime has been studied in pneumatic [16] and hydraulic conveying systems [18] experimentally and numerically [1]. It would be of great interest to revisit these regimes, which here are referred to as pseudoplug as they seem to correspond to precursors of plugs, with the physical approach developed for studying geophysical dunes [19,20]. Experimental observations with close-up images captured and analysis should help clarify this.

Plug traveling velocities and lengths were statistically studied for various imposed water flow rate values. Plug and pseudoplug velocity distributions centered around the median traveling velocity appeared to correspond to a very steep distribution and a uniform distribution with two extrema,

respectively. The averaged flow velocity calculated with the half-filled tube assumption seems to correspond to the median velocity determining the plugs' velocity distribution. In the case of pseudoplug, the median velocity that determines the width of the uniform distribution as well as its center corresponds to the average flow velocity in the tube with a decreasing filling fraction as the increasing imposed flow rate is responsible for an increasing erosion of the sedimented bed.

The plug length distribution has been seen to follow a log-normal distribution, which is typical for random splitting processes. Here the median value and its variance increase as the flow rate increases. This statistical observation could help future modeling approaches explain the plug formation process.

Our experimental results expand numerical observations showing an increase in the plugs' lengths and the speed of the front plugs as the superficial velocity increases [39], with a statistical approach made possible with the large number of plugs studied. The effect of the flow rate on the pressure drop of the water-solid flow has also been studied. An asymptotic trend towards solid-free fluid flow has been recovered for high flow rate values due to the increasing dilution of the solid whose mass rate remains fixed while the fluid flow rate increases. In the pseudoplug regime, the fluidization of the granular matter allowed us to use filling-fraction-dependent effective viscosity models for granular suspension in order to obtain a good predictor of the pressure drop. The pressure drop measurements in the plug regime resist a simple modeling which considers solid friction at the interface between plugs and the tube's wall, and viscous dissipation between two plugs. A more detailed modeling taking into account a tribological description at the interface between the traveling plug and the tube's wall together with a stress redirection within the granular material inside the plug and the viscous drag seems to be necessary here [37].

Further experimental observations with different hydraulic or pneumatic conveying systems would be of great interest to expand and give corrections to the present model. This work on hydraulic conveying of glass beads in a millifluidic tube has shown interesting analogies with pneumatic conveying of granular materials. In the future it would be of great interest to delve into the analogies and differences between the two systems as some unifying laws could be discovered [16,21].

E.G. conducted and interpreted the experiments, M.F. developed and applied the statistical methodology, and G.D. supervised the whole project.

-
- [1] M. Zhou, S. Kuang, K. Luo, R. Zou, S. Wang, and A. Yu, *Powder Technol.* **373**, 543 (2020).
 - [2] Z. Li-an, C. Ronghuan, and W. Tieli, *IOP Conf. Ser.: Earth Envir. Sci.* **113**, 012163 (2018).
 - [3] N. Kumar, M. K. Gopaliya, and D. Kaushal, *Part. Sci. Technol.* **37**, 232 (2019).
 - [4] X. Li, L. Guo, and W. Xu, *J. Phys.: Conf. Ser.* **1626**, 012179 (2020).
 - [5] R. Rani and M. K. Jain, *Part. Sci. Technol.* **37**, 123 (2019).
 - [6] L. Pullum, D. V. Boger, and F. Sofra, *Annu. Rev. Fluid Mech.* **50**, 157 (2018).

- [7] F. Osanloo, M. R. Kolahchi, S. McNamara, and H. J. Herrmann, *Phys. Rev. E* **78**, 011301 (2008).
- [8] M. Houssais, C. P. Ortiz, D. J. Durian, and D. J. Jerolmack, *Phys. Rev. E* **94**, 062609 (2016).
- [9] R. M. Ashley and M. A. Verbanck, *J. Hydraul. Res.* **34**, 753 (1996).
- [10] B. C. O’Kelly, *Proceedings of the Institution of Civil Engineers. Municipal Engineer* (Telford, London, 2004), Vol. 157, pp. 193–197.
- [11] R. Durand, *Proceedings of the International Association for Hydraulic Research, Fifth Congress* (IAHR, Minneapolis, 1953), pp. 89–103.
- [12] R. D. M. Newitt, J. F. Richardson, M. Abbott, and R. B. Turtle, *Trans. Inst. Chem. Eng.* **33**, 293 (1955).
- [13] K. C. Wilson, G. R. Addie, A. Sellgren, and R. Clift, *Slurry Transport Using Centrifugal Pumps* (Springer, New York, 2006).
- [14] A. Uzi and A. Levy, *Powder Technol.* **326**, 302 (2018).
- [15] B. Ismael, *Fluid- und Feststofftransport in Rohrsystemen und Pumpstationen* (Technische Universität Dresden, Dresden, 2021).
- [16] H. Kalman and A. Rawat, *Chem. Eng. Sci.* **211**, 115256 (2020).
- [17] E. Rabinovich and H. Kalman, *Powder Technol.* **207**, 119 (2011).
- [18] L. A. Borzone, *Chem. Eng. Commun.* **197**, 1215 (2010).
- [19] F. Charru, B. Andreotti, and P. Claudin, *Annu. Rev. Fluid Mech.* **45**, 469 (2013).
- [20] M. Ouriemi, P. Aussillous, and E. Guazzelli, *J. Fluid Mech.* **636**, 321 (2009).
- [21] H. Kalman, D. Portnikov, O. G. Gabrieli, and N. M. Tripathi, *Powder Technol.* **354**, 485 (2019).
- [22] M. do Carmo Ferreira, J. T. Freire, and G. Massarani, *Powder Technol.* **108**, 46 (2000).
- [23] O. Orozovic, A. Lavrinec, Y. Alkassar, K. Williams, M. G. Jones, and G. Klinzing, *Powder Technol.* **351**, 84 (2019).
- [24] J. Li, C. Webb, S. S. Pandiella, G. M. Campbell, T. Dyakowski, A. Cowell, and D. McGlinchey, *Chem. Eng. Process.* **44**, 167 (2005).
- [25] S. Shaul and H. Kalman, *Powder Technol.* **272**, 322 (2015).
- [26] P. Vlasák, Z. Chara, J. Krupicka, and J. Konfrst, *J. Hydrol. Hydromech.* **62**, 241 (2014).
- [27] L. Wang, A. Goharzadeh, and P. Rodgers, *AIP Conf. Proc.* **1376**, 351 (2011).
- [28] Z. Chara, P. Vlasak, J. Konfrst, and B. Kysela, *AIP Conf. Proc.* **1648**, 030021 (2015).
- [29] E. Papista, D. Dimitrakakis, and S. G. Yiantsios, *Ind. Eng. Chem. Res.* **50**, 630 (2011).
- [30] J. J. Stickel and R. L. Powell, *Annu. Rev. Fluid Mech.* **37**, 129 (2005).
- [31] E. Guazzelli and O. Pouliquen, *J. Fluid Mech.* **852**, P1 (2018).
- [32] D. J. Jerolmack and K. E. Daniels, *Nat. Rev. Phys.* **1**, 716 (2019).
- [33] C. Pierlot, H. Hu, C. Reeb, J. Bassetti, M. Bertin, D. Lambertin, C. Davy, and V. Nardello-Rataj, *Chem. Eng. Sci.* **255**, 117635 (2022).
- [34] H. B. Mann and D. R. Whitney, *Ann. Math. Stat.* **18**, 50 (1947).
- [35] A. N. Kolmogorov, *Dokl. Akad. Nauk SSSR* **31**, 99 (1941).
- [36] A. F. Filippov, *Theory Probab. Appl.* **6**, 275 (1961).
- [37] S. Shaul and H. Kalman, *Powder Technol.* **256**, 310 (2014).
- [38] S. Ergun, *Chem. Eng. Prog.* **48**, 89 (1952).
- [39] S. B. Kuang, K. W. Chu, A. B. Yu, Z. S. Zou, and Y. Q. Feng, *Ind. Eng. Chem. Res.* **47**, 470 (2008).